JACS
JOURNAL OF THE AMERICAN CHEMICAL SOCIETY
pubs.acs.org/JACS
Article

Synthesis and In Situ Thermal Induction of β-Sheet Nanocrystals in Spider Silk-Inspired Copolypeptides

Tianjian Yang,† Tianrui Xue,† Jianan Mao, Stephen R. Ekatan, Yingying Chen, Ziyuan Song, Jianjun Cheng,* and Yao Lin*

Cite This: https://doi.org/10.1021/jacs.4c10998
Read Online
ACCESS | Metrics & More | Article Recommendations | Supporting Information

ABSTRACT: Spider silk, known for its exceptional tensile strength, extensibility, and toughness, continues to inspire advancements in polymer and materials science. Despite extensive research, synthesizing materials that encompass all these properties remains a significant challenge. This study addresses this challenge by developing high molecular-weight multiblock synthetic copolypeptides that mimic the hierarchical structure and mechanical properties of spider silk. Using autoaccelerated ring-opening polymerization of *N*-carboxyanhydrides, we synthesized copolypeptides featuring transformable β-sheet blocks. These blocks retain a helical structure during synthesis but transition into β-sheet nanocrystals in situ during solvent-free thermal mechanical processing. Compression molding was employed to induce hierarchical ordering within the copolypeptide films, resulting in a solid "liquid crystalline" structure that undergoes a temperature-induced α-to-β structural transformation. This transformation integrates β-sheet nanocrystals throughout the helical block matrix, significantly enhancing the material's mechanical performance. Our innovative synthesis and processing strategy, which involves alternating sequences of α-helical and β-sheet blocks with various β-sheet-forming NCAs, enables the customization of diverse mechanical characteristics. These advancements not only deepen our understanding of the fundamental design principles of spider silk but also pave the way for a new generation of high-performance, silk-inspired synthetic copolypeptides with broad application potential.

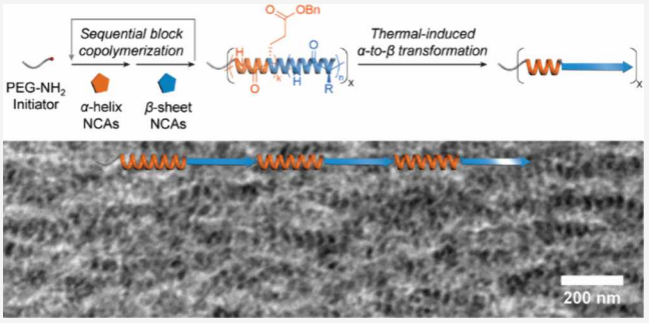

INTRODUCTION

Spider silk is renowned as nature's high-performance protein fiber, distinguished by its excellent tensile strength, extensibility, and toughness. This unique combination of mechanical properties has spurred extensive research into the structural-property relationship of spider silk,[1−6] with the goal of leveraging these insights to develop reconstituted,[7−16] artificial,[17−20] or silk-inspired materials[21−27] that could potentially surpass the mechanical capabilities of their natural counterparts. Over recent decades, focused research on spider dragline silk has led to significant advancements in understanding its intricate molecular architecture and fundamental design principles.[28−37] These advancements have been facilitated by methodologies such as solid-state nuclear magnetic resonance (NMR) spectroscopy,[28−30] advanced molecular simulations,[31−33] and innovative techniques for precise mechanical property quantification.[34−36]

Critical design features that contribute to spider silk's superior performance include its hierarchical structure, which arises from a complex synthesis, morphology and process controls. For instance, Spidroin I and II are high molecular weight (MW) polypeptides characterized by distinct poly alanine (poly-Ala) blocks interspersed with glycine-rich (Gly) regions.[2,28] The mechanical strength of the silk is largely attributed to antiparallel β-sheet nanocrystals formed during the spinning process, primarily consisting of poly-Ala and poly(Gly-Ala) sequences.[5,6,30,34] These nanoscale structures act as stiff cross-linking domains within a semiamorphous matrix. The matrix, featuring less structured β-configurations and helical structures with trifold symmetry primarily formed by glycine residues, also plays a crucial role in dictating the silk's mechanical properties.[28,29] Remarkably, reducing the size of the β-sheet nanocrystals correlates with increased material toughness and enhanced ultimate strength.[31,34] Additionally, the ability of spiders to produce more than seven distinct types of silk,[1] each with unique properties, highlights the versatility and the sophisticated biological engineering inherent in spider silk production. Seldom can a synthetic polymer platform

Received: August 11, 2024
Revised: October 24, 2024
Accepted: October 25, 2024

Scheme 1. Schematic Representation of the Synthesis of Spider Silk-Inspired Polypeptide Materials via Controlled Multiblock Copolypeptide Synthesis, Solvent-Free Thermal Processing, and In Situ Thermal Induction of β-Sheet Formation

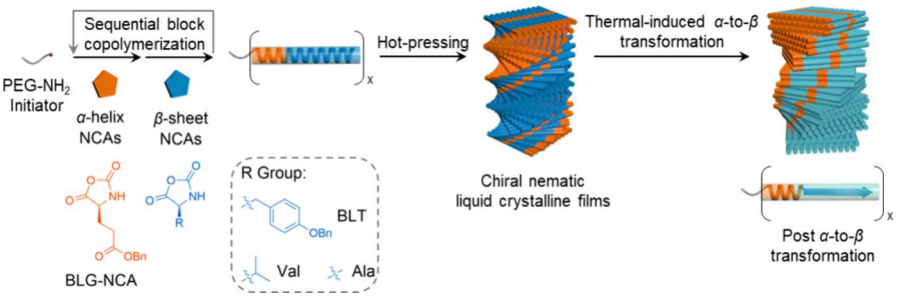

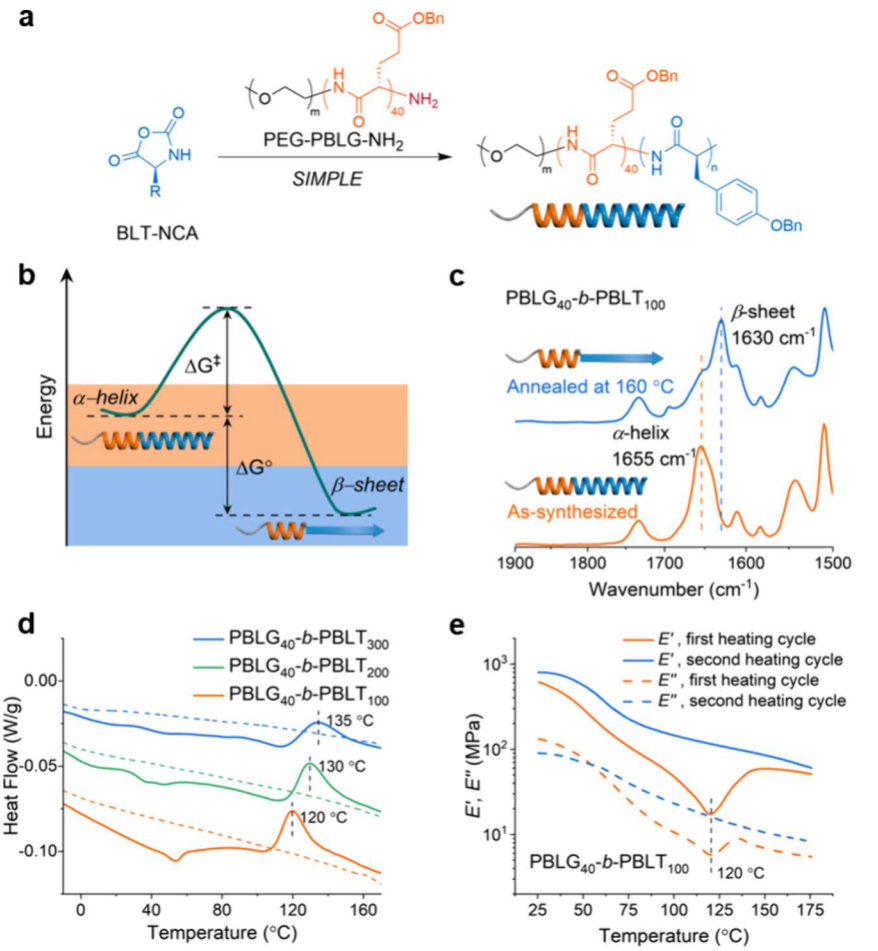

Figure 1. Synthesis of block copolypeptides and temperature-induced α-helix to β-sheet transformation in the solid state. (a) Schematic representation of the synthetic route for PBLT-based β-sheet-forming block copolypeptides, initially confined in an α-helical conformation, using the SIMPLE polymerization method with a helical PBLG macroinitiator. (b) Schematic representation of the free energy diagram illustrating the α-to-β transition experienced by PBLT in the block copolypeptides. (c) FTIR-ATR spectra of the PBLG$_{40}$-*b*-PBLT$_{100}$ before and after α-to-β transition, induced by temperature. (d) DSC profiles of as-synthesized PBLG$_{40}$-*b*-PBLT$_n$ with various PBLT chain lengths. Solid lines indicate the first heating cycles, while dashed lines represent the second heating cycles. Heating rate: 3 °C/min. (e) DMTA profiles of PBLG$_{40}$-*b*-PBLT$_{100}$ films before and after the α-to-β transition, demonstrating the thermal-hardening effect. Heating rate: 3 °C/min.

match the combination of tensile strength, extensibility, processability, and versatility found in spider silk.

Building on these discoveries, our study seeks to bridge the gap between the natural marvel of spider silk and the domain of synthetic biopolymers, specifically those with well-defined secondary structures, such as synthetic polypeptides prepared through ring-opening polymerization of amino acid *N*-carboxyanhydrides (ROP-NCAs).[38−42] By investigating high MW multiblock synthetic copolypeptides and employing the latest technique of autoaccelerated ROP-NCAs,[43−50] we aim to replicate the hierarchical structure and the intricate balance of order and disorder in chain configurations that endow spider silk with its remarkable mechanical properties. A distinctive feature of our methodology is the incorporation of transformable β-sheet blocks, which retain a helical structure during synthesis but transition into β-sheet nanocrystals in situ during thermomechanical processing. This solvent-free transformation is crucial for achieving the hierarchical ordering observed in

https://doi.org/10.1021/jacs.4c10998
J. Am. Chem. Soc. XXXX, XXX, XXX−XXX

natural spider silk, with significant scale-up potential. Moreover, our methodology allows for precise control over the chemical domains, enabling the fine-tuning of mechanical properties across a wide spectrum. This control not only enhance the material's mechanical performance but also expands the potential applications of these silk-inspired synthetic polypeptides.

Our design, illustrated in Scheme 1, represents a significant advancement over previous studies employing multiblock polypeptides. First, by leveraging the autoaccelerated helical chain growth of NCA monomers through a cooperative polymerization mechanism,[44,45,51] we have achieved fast and precise incorporation of β-sheet-forming NCAs, such as *O*-benzyl-L-tyrosine (BLT) NCA.[52] This methodology maintains the polymer chains in a helical configuration alongside leading helical blocks, like poly(benzyl-L-glutamate) (PBLG), preventing premature chain termination and polymer segregation common in the synthesis of β-sheet polypeptides. This innovation facilitates streamlined processing postsynthesis. Second, we utilize thermomechanical processing techniques, such as compression molding, to directly convert the synthesized copolypeptides (e.g., PBLG-*b*-PBLT) into films with hierarchical ordering. Within these films, the helical copolypeptides form a unique solid "liquid crystalline" structure (e.g., chiral nematic),[53−55] as illustrated in Scheme 1. This structure is further refined by applying heat to induce an α-to-β structural transformation in the PBLT blocks, resulting in the distribution of β-sheet nanocrystals throughout the helical PBLG matrix. Lastly, our synthesis and processing strategy is highly adaptable, suitable for sequences alternating between α-helix and β-sheet blocks, with the capability for up to four repeats, as demonstrated in this study. This versatility extends to a broad range of β-sheet-forming NCAs, including L-alanine (Ala) and L-valine (Val) NCAs.[56−58] Such adaptability provides precise control over the mechanical properties of synthetic materials. The combination of precision synthesis, remarkable tunability, and compatibility with industrial processing methods underscores the potential of this research to create a new class of high-performance, silk-like synthetic polymers.

RESULTS AND DISSCUSION

Synthesis of β-Sheet-Forming Block Copolypeptides Confined under α-Helical Conformation. Efforts to develop synthetic polypeptides capable of transitioning between α-helix and β-sheet structures in the solid state have been ongoing since the 1950s but have achieved limited success.[52,59−64] Polypeptides predisposed to form β-sheets often aggregate and halt chain growth prematurely during synthesis, complicating the production of high MW polypeptides in large quantities.[21,56,65−67] Conversely, polypeptides less prone to β-sheet formation require very demanding processing conditions—such as simultaneous heating, swelling, and stretching—to facilitate structural transformations, often resulting in low success rates.[60,61]

Our method utilizes the autoaccelerated, helical growth of polypeptide chains formed by NCAs through a cooperative polymerization mechanism.[44,45,51] In previous studies, we successfully integrated several β-sheet-prone NCAs with helical NCAs in a random copolymerization process, using an α-helical PBLG as a guiding scaffold.[68,69] The approach incorporates β-sheet-prone NCAs such as BLT-NCA, Val-NCA, and Ala-NCA, confining them within an α-helical structure due to the activation energy barriers[70−72] associated with switching configurations. After synthesis, α-to-β structural transformations can be induced by changes in temperature or solvent conditions.

Extending this approach to block copolypeptides, we employed a PEG−PBLG$_{40}$ macroinitiator to initiate the ring-opening polymerization of BLT-NCA with accelerated reaction kinetics, controlling the polymerization of PBLT blocks at various monomer-to-initiator (M/I) ratios in a water/dichloromethane (DCM) biphasic system (Figure 1a). This method uses our previously developed SIMPLE (Segregation-Induced Monomer-Purification and initiator-Localization promoted rate-Enhancement) method.[45,68] The resulting PBLG$_{40}$-*b*-PBLT$_n$ block copolypeptides, with "*n*" indicating the degree of polymerization (DP) of the PBLT segment (n = 100, 200 and 300), retained α-helical structures after polymerization in DCM (Figure S3). Following the reaction, the DCM solution containing the polypeptides was precipitated into a mix of hexane and ethyl ether, then washed and vacuum-dried. These copolypeptides demonstrated a controlled DP and precise composition, as confirmed by NMR (Table S1 and Figures S33−S35). Detailed synthesis procedures, GPC, and ^{1}H NMR characterizations of these macromolecules are provided in the Supporting Information (Materials and Methods, Figures S1 and S2, and Table S1).

The PBLT block in PBLG$_{40}$-*b*-PBLT$_n$ undergoes a transformation from its initial α-helical conformation to a β-sheet structure upon heating, due to PBLT's propensity to form thermodynamically more favorable β-sheets (Figure 1b). Initially, the helical state after synthesis is confirmed by the characteristic α-helix peak at 1655 cm^{-1}, as identified by attenuated total reflectance Fourier-transform infrared spectroscopy (ATR-FTIR) (Figure 1c and Figure S4). Upon heating above 110 °C, the sample undergoes a conformational transition, forming β-sheets as indicated by the emergence of a new amide I peak at 1630 cm^{-1} (Figure 1c). Differential scanning calorimetry (DSC) analysis (Figure 1d and Figure S5) reveals an endothermic peak at around 50 °C during the first heating cycle, corresponding to the melting of the short PEG segment introduced from the macroinitiator,[73,74] followed by a significant exothermic peak above 110 °C, signifying the PBLT's transition to a β-sheet configuration—a finding corroborated by FTIR analyses. The absence of phase transitions during the second heating suggests the permanence of this transformation (Figure 1d). When tested on samples of different lengths of PBLT blocks, the exothermic peaks associated with the α-helix to β-sheet transition are broader and occur at higher temperatures for PBLG$_{40}$-*b*-PBLT$_n$ with higher n (Figure 1d).

The α-helix to β-sheet conversion within the copolypeptide is irreversible and is achieved through simple heating, resulting in a substantial alteration of the material's structure. The formation of β-sheets between PBLT chains creates a stable interlocking network that prevents the PEG segment from recrystallizing (Figure 1d). Dynamic mechanical thermal analysis (DMTA) conducted on films prepared from compression molding of PBLG$_{40}$-*b*-PBLT$_{100}$ at 80 °C, both pre- and post-thermal induction of the α-to-β transformation (Figure 1e, first and second heating cycles, respectively), corroborates the structural shift. The DMTA results for PBLG$_{40}$-*b*-PBLT$_{200}$ and PBLG$_{40}$-*b*-PBLT$_{300}$ further confirm that the transformation yields a material with an elevated modulus, enhancing mechanical integrity and its capacity to

https://doi.org/10.1021/jacs.4c10998
J. Am. Chem. Soc. XXXX, XXX, XXX−XXX

endure higher temperatures (Figure S6). This mechanical reinforcement, as evidenced by the DMTA, underscores the potential of thermally induced β-sheet formation in enhancing the structural robustness of polymer materials.

Thermomechanical Processing for Controlled β-Sheet Transformation in the Solid State. Once formed within polypeptides, β-sheet structures are often incompatible with standard thermomechanical processing techniques such as compression molding or extrusion due to the intermolecular H-bonds acting as physical cross-links, which limit polymer processability.[61] When processing β-sheet polypeptides into materials via solution methods, the dense network of hydrogen bonds often necessitates the use of aggressive and potentially hazardous reagents to disrupt these bonds.[9,12−14] In contrast, α-helical polypeptides, with their rod-like architectures and weak interactions, offer significantly better thermal processability, facilitating 'slipping' under heat and pressure.[61,75,76] Moreover, their predisposition to form cholesteric or nematic liquid crystalline structures enhances processability and promotes cooperativity in structural transitions through long-range supramolecular ordering.[53−55]

Our findings confirm that the as-synthesized helical state of the copolypeptides grants these materials exceptional processability. When PBLG$_{40}$-*b*-PBLT$_{100}$ powders are hot-pressed at 80 °C between Kapton films, they form uniform, clear films (inset of Figure 2a). The PEG segment, incorporated through SIMPLE polymerization, acts as a plasticizer when melted at this temperature, enhancing the malleability of the helical copolypeptides. FTIR-ATR and wide-angle X-ray diffraction (WAXD) analyses confirm that the films predominantly retain the α-helical structure (Figure 2c,d).[52,76−80] Polarized optical microscope (POM) images of the PBLG$_{40}$-*b*-PBLT$_{100}$ films reveal strong birefringence both before and after the α-to-β transition (Figure 2a,b), induced by thermal annealing at 160 °C for 15 min. The fingerprint textures observed at higher magnifications (Figure S7) suggest the chiral nematic nature of these solid 'liquid crystalline' materials, similar to the hot-pressed PBLG films we previously studied.[55]

FTIR and WAXD confirm that a brief annealing of PBLG$_{40}$-*b*-PBLT$_{100}$ films at 160 °C for 15 min leads to approximately 88% conversion of PBLT$_{100}$ to β-sheets (Figure 2c,d and Figure S8). Lower annealing temperatures, such as 110 °C for 5 or 15 min, achieve lesser conversions—around 54 and 68%, respectively. Temperature-controlled X-ray diffraction (XRD) was applied to monitor the structure evolution from α-helical to β-sheet conformation in situ (Figure S9), confirming the findings from WAXD.

Tensile tests on PBLG$_{40}$-*b*-PBLT$_{100}$ films with varying β-sheet content reveal a positive correlation between increased β-sheet percentage and mechanical strength at room temperature (Figure 2e, Figure S10, and Table S3). For example, films from hot-pressing at 80 °C exhibited an ultimate tensile strength (σ) of ∼4 MPa and a Young's modulus (E) of ∼360 MPa, whereas films annealed at 160 °C for 15 min with 88% β-sheet conversion showed doubled σ (∼10 MPa) and increased E (∼580 MPa). Post α-to-β transition, a slight reduction in ductility—from ∼13 to ∼8%—is noted, attributed to the limited plastic deformation of the now physically cross-linked polypeptide network. At 100 °C, the tensile discrepancy between α-helix and β-sheet films becomes even more pronounced (Figure 2f), with the films with 88% β-sheet conversion showing σ and E values (∼4.8 and ∼150 MPa) far surpassing those of the α-helix films (∼0.4 and ∼25 MPa).

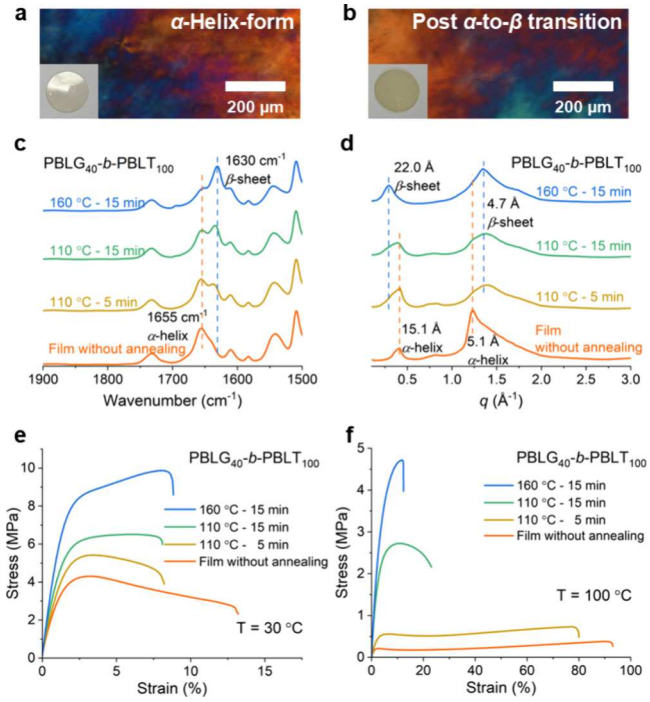

Figure 2. Comparative analysis of morphological structures and mechanical properties of PBLG-*b*-PBLT block copolypeptides before and after α-to-β transition. (a) POM images illustrating the surface of PBLG$_{40}$-*b*-PBLT$_{100}$ films in α-helix form. (b) POM images of the same films after the α-to-β transition induced by annealing at 160 °C. Insets in (a) and (b): photographs showing the films' appearance before and after the transition. (c) ATR-FTIR spectra of PBLG$_{40}$-*b*-PBLT$_{100}$ films processed under different thermal conditions, demonstrating structural changes. (d) WAXD patterns of the same films, highlighting the crystalline transformations associated with thermal processing. (e, f) Tensile stress−strain curves of PBLG$_{40}$-*b*-PBLT$_{100}$ films, measured at 30 and 100 °C, respectively, to evaluate mechanical properties under different thermal processing histories. PBLG$_{40}$-*b*-PBLT$_{100}$ films without annealing were prepared by hot-pressing at 80 °C.

This significant tensile modulus enhancement at elevated temperatures following the α-to-β transition was corroborated by earlier DMTA results (Figure 1e).

The in situ generation of β-sheets via a straightforward temperature-induced α-to-β transition in the solid state significantly reinforces the polymer network, enhancing the thermal-mechanical stability of polypeptide materials. PBLG-*b*-PBLT serves as a model system for this controlled modulation of material properties. Inspired by the multiblock architecture of dragline silk, we then synthesized sequences with alternating α-helix and β-sheet blocks, aiming to improve both ultimate tensile strength and the extensibility of the copolypeptides materials. By incorporating longer chains that potentially participate in multiple β-sheet nanocrystals, we expect to create a more cohesive and resilient polymer network.

Enhancing Mechanical Performance with Multiblock Copolypeptides and Repetitive β-Sheet Segments. Utilizing the SIMPLE living polymerization technique,[45,46] we synthesized multiblock copolypeptides designated as (PBLG$_{40}$-*b*-PBLT$_{200}$)$_x$, with "x" varying from 1 to 4 to represent the number of repeating blocks. The DP for PBLT blocks was designed to be around 200 to increase the chain lengths. Detailed synthesis procedures and ^{1}H NMR characterizations of these polymers are provided in the SI (Materials

https://doi.org/10.1021/jacs.4c10998
J. Am. Chem. Soc. XXXX, XXX, XXX−XXX

and Methods, Table S1, and Figures S35−S38). These copolypeptides maintained their designed α-helical conformation postsynthesis (Figure S11). For polymer film preparation, we applied a hot-press at 160 °C and followed by an hour of annealing to facilitate the α-to-β transition. This process produced uniform films across all polymer variants, with ATR-FTIR and WAXD confirming the formation of β-sheets (Figure 3b and Figure S12). FTIR peak deconvolution

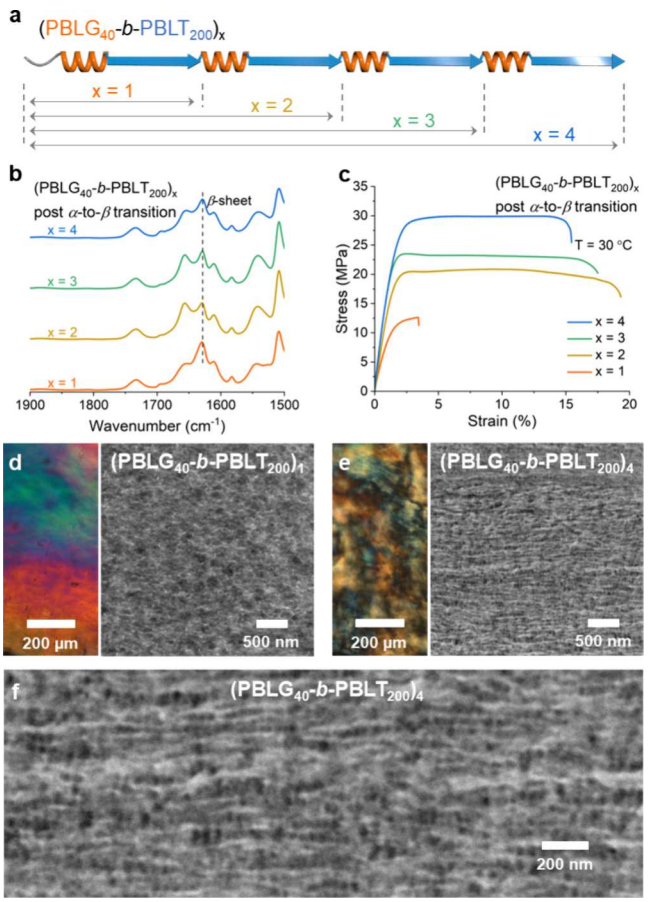

Figure 3. Mechanical performance and morphology of $(PBLG_{40}\text{-}b\text{-}PBLT_{200})_x$ multiblock copolypeptides with in situ formed β-sheet nanocrystals. (a) Schematic of the designed $(PBLG_{40}\text{-}b\text{-}PBLT_{200})_x$ multiblock copolypeptides, varying by the number of repeating blocks. (b) FTIR-ATR spectra of the multiblock copolypeptide films following in situ α-to-β transition, exhibiting structural changes. (c) Tensile stress−strain curves of $(PBLG_{40}\text{-}b\text{-}PBLT_{200})_x$ films at 30 °C, showing variations in mechanical properties across different block configurations. (d, e) POM (left) and TEM (right) images showing the surfaces and microtome sections of $(PBLG_{40}\text{-}b\text{-}PBLT_{200})_1$ and $(PBLG_{40}\text{-}b\text{-}PBLT_{200})_4$ films, respectively, showing surface details and cross-sectional nanostructures. (f) High-magnification TEM image of the microtome sections of $(PBLG_{40}\text{-}b\text{-}PBLT_{200})_4$ film, showing the distribution of β-sheet nanocrystals (dark domains) and the resulting network. The films were fabricated through hot-pressing at 160 °C to achieve maximum α-to-β conversion.

revealed a β-sheet conversion of 55−70% in the $PBLT_{200}$ segments (Figure S13 and Table S2). Room temperature tensile tests showed significant mechanical enhancements with the number of repeating blocks; ultimate tensile strength tripled to approximately 30 MPa, and Young's modulus doubled to about 2 GPa in $(PBLG_{40}\text{-}b\text{-}PBLT_{200})_4$ compared to $(PBLG_{40}\text{-}b\text{-}PBLT_{200})_1$ (Figure 3c, Table 1, and Figure S14). Additionally, ductility improved, likely due to the entanglement effect from the multiblock design, which fortified the polymer network.

Morphological analyses were conducted to understand the influence of the multiblock architecture on material nanostructures and resultant macroscopic properties. POM studies indicated a transition from cholesteric to almost nematic supramolecular organization as the number of blocks increased from $x = 1$ to $x = 4$ (Figure 3d,e and Figure S15). TEM cross sections revealed the formation of more uniformly distributed β-sheet crystals in $(PBLG_{40}\text{-}b\text{-}PBLT_{200})_4$, presenting as dark nanometer-scale domains within an interlaced network, measured with approximately 28−42 nm in size (Figure 3e,f and Figure S16c,d). This contrasted with the less regular β-sheet domains in films of $(PBLG_{40}\text{-}b\text{-}PBLT_{200})_1$ (Figure 3d and Figure S16a,b). The well-integrated network observed in $(PBLG_{40}\text{-}b\text{-}PBLT_{200})_4$ significantly enhances the material's ultimate tensile strength and modulus.

In the $(PBLG_{40}\text{-}b\text{-}PBLT_{200})_x$ polymer series, despite the multiblock architecture leading to increased extensibility, the elongation at break remains relatively low, not exceeding 20%. This observation prompted us to draw inspiration from spider silk, where β-sheet crystals typically make up less than 20% of the structure and are embedded within a matrix of structured but less ordered domains.[81] Motivated by this, we increased the proportion of PBLG domains, hypothesizing that elongating the α-helical segments would decrease the β-sheet domain sizes due to a reduced probability of adjacent PBLT block alignment necessary for β-sheet formation.

Optimized Multiblock Copolypeptides with Smaller β-Sheet Nanodomains: Balancing Strength and Ductility. The strategic modification of the $(PBLG_{200}\text{-}b\text{-}PBLT_{200})_x$ series, with "x" ranging from 1 to 3, has significantly enhanced the ductility of the materials by extending the α-helical PBLG segments (Figure 4). Detailed synthesis procedures and ^1H NMR characterizations of the polymers are provided in the SI (Materials and Methods, Table S1, and Figures S39−S41). These copolypeptides maintained α-helical conformation postsynthesis (Figure S17). This adjustment has been crucial in achieving an optimal balance between strength and toughness. As the number of repetitive blocks increased from 1 to 3, the β-sheet content in the materials decreased from 38 to 31% (Figure 4b, Figures S18 and S19, and Table S2), corresponding with substantial gains in material performance: elongation at break increased from approximately 45 to 80%, and ultimate tensile strength rose from about 13 to 23 MPa (Figure 4c, Figure S20, and Table 1).

Morphological analyses highlighted a shift from cholesteric to nematic organizational patterns in the polymers with more repetitive blocks, as evidenced by POM (Figure 4d,e and Figure S21). TEM studies revealed that $(PBLG_{200}\text{-}b\text{-}PBLT_{200})_3$ featured a consistently dispersed nanodomain lattice about 13−20 nm in size within the nematic layers (Figure 4e,f and Figure S22c,d). Remarkably, these domains were roughly half the size of those in $(PBLG_{40}\text{-}b\text{-}PBLT_{200})_4$, suggesting enhanced interdomain connectivity that likely facilitates macromolecular threading across structural domains. This connectivity is expected to inhibit crack propagation and enhance the polymer network's integrity, as supported by tensile testing results.

The strain hardening exhibited by films from $(PBLG_{200}\text{-}b\text{-}PBLT_{200})_2$ and $(PBLG_{200}\text{-}b\text{-}PBLT_{200})_3$ (Figure 4c) suggests a potential transformation mechanism within the PBLT in the less structured matrix, as more than 30% of PBLT strands are

https://doi.org/10.1021/jacs.4c10998
J. Am. Chem. Soc. XXXX, XXX, XXX−XXX

Table 1. Summary of the Mechanical Properties of Multiblock Copolypeptide Materials Tested at 30 °C[b]

entry	composition	α-to-β conversion[a]	E (MPa)	σ (MPa)	ε (%)
1	$PBLG_{40}$-*b*-$PBLT_{200}$	69%	920 ± 50	11.6 ± 0.9	2 ± 1
2	$(PBLG_{40}$-*b*-$PBLT_{200})_2$	56%	1450 ± 190	20.0 ± 0.9	14 ± 7
3	$(PBLG_{40}$-*b*-$PBLT_{200})_3$	57%	2000 ± 240	23.6 ± 3.0	16 ± 2
4	$(PBLG_{40}$-*b*-$PBLT_{200})_4$	62%	2210 ± 230	29.7 ± 0.6	12 ± 3
5	$PBLG_{200}$-*b*-$PBLT_{200}$	76%	990 ± 100	14.2 ± 1.1	56 ± 11
6	$(PBLG_{200}$-*b*-$PBLT_{200})_2$	68%	1330 ± 250	19.1 ± 2.0	70 ± 7
7	$(PBLG_{200}$-*b*-$PBLT_{200})_3$	63%	1510 ± 160	23.3 ± 1.8	86 ± 14
8	$PBLG_{40}$-*b*-$PVal_{30}$	89%	660 ± 20	10.2 ± 0.2	6 ± 1
9	$(PBLG_{40}$-*b*-$PVal_{30})_2$	91%	840 ± 200	13.2 ± 0.2	9 ± 1
10	$(PBLG_{40}$-*b*-$PVal_{30})_3$	78%	1520 ± 400	21.7 ± 0.6	13 ± 1
11	$PBLG_{40}$-*b*-$PAla_{100}$	32%	240 ± 40	5.1 ± 0.4	33 ± 5
12	$(PBLG_{40}$-*b*-$PAla_{100})_2$	56%	1650 ± 190	26.0 ± 2.8	18 ± 9

[a]The α-to-β conversion values for PBLT, PVal, and PAla were determined from peak deconvolution of FTIR spectra. [b]Data represent the mean of at least three replicate experiments. E: Young's modulus measured at 30 °C. σ: Ultimate tensile strength measured at 30 °C. ε: Elongation at break measured at 30 °C.

not initially incorporated into β-sheet nanocrystals. During stretching, some of these strands likely reorganize with neighboring strands into β-sheets, aligning and locking together through interstrand hydrogen bonds under the applied tension. This reconfiguration organizes polymer chains into structures with enhanced intermolecular interactions, thereby increasing the material's resistance to further deformation. More pronounced strain hardening was observed in these samples during tensile tests conducted at 100 °C (Figure S23a,b)—a condition that enhances chain "slipping". A similar phenomenon was also found in $(PBLG_{40}$-*b*-$PBLT_{200})_4$ under the same conditions (Figure S23c,d). Although this mechanism requires further validation, it implies that the initial reduction of β-sheet formation in unstressed conditions may provide a 'reserve' of structural reorganization potential, which can be activated upon stretching. This adaptive reconfiguration of molecular structure under stress underscores the dynamic potential of multiblock copolypeptide materials, signifying their capacity for mechanical adaptation—an essential attribute for applications aiming to mimic the remarkable properties of natural spider silk.

Tailoring Mechanical Profiles with β-Sheet-Forming Amino Acids. Spider silk's diverse amino acid composition enables a broad spectrum of mechanical properties, each tailored to specific functional needs. Utilizing advanced helical ROP-NCA techniques, we have expanded the chemical domains of block copolypeptides by incorporating β-sheet-forming amino acids like valine (Val) and alanine (Ala), which are known for their distinct folding propensities (Figure 5a,d).[56−58] The detailed synthesis procedures and ^{1}H NMR characterizations of these polymers are provided in the SI (Materials and Methods, Table S1, and Figures S42−S46).

Similar to the trends observed in longer-chain (PBLG-*b*-PBLT)$_x$ polymers, $(PBLG_{40}$-*b*-$PVal_{30})_x$ (x = 1, 2, and 3) copolypeptide films exhibited controlled temperature-induced α-to-β transformation as evidenced by FTIR and WAXS, with a β-sheet conversion of 80−90% in the $PVal_{30}$ segments (Figure 5b, Figures S24 and S25, and Table S2). This led to the enhancement of material properties and morphological tunability as the number of repeating blocks increases from 1 to 3 (Figure 5c and Figure S26). This outcome is particularly noteworthy given the relatively short polymer chain length, even for $(PBLG_{40}$-*b*-$PVal_{30})_3$. Further investigations into $(PBLG_{40}$-*b*-$PAla_{100})_x$ (x = 1 and 2), as illustrated in Figure 5e,f, underscore the versatility of our synthetic and processing strategy. Interestingly, in multiblock architectures, the PAla block of $(PBLG_{40}$-*b*-$PAla_{100})_2$ shows a significantly higher yield of α-to-β transformation compared to $(PBLG_{40}$-*b*-$PAla_{100})_1$ (Figure 5e and Figures S27 and S28), resulting in an approximately 5-fold increase in ultimate strength (Figure 5f). A detailed comparison of mechanical benchmarks—ultimate strength, extensibility, and tensile modulus—across various copolypeptide compositions and from multiple measurements is summarized in Table 1.

Table 1 demonstrates that, generally, tensile modulus, ultimate strength, and extensibility increase with the number of repeating blocks in the same copolypeptide compositions. This trend is primarily attributed to the multiblock design and the formation of β-sheet nanostructures, rather than merely to an increase in the molecular weight of the polypeptide chains. To prove this, we synthesized random copolypeptides of $P(BLG_{0.5}$-*r*-$BLT_{0.5})_{1200}$ (Figure S29a), comprising 50% BLG and 50% BLT residues, with a total degree of polymerization of 1200, as a control group. Contrary to the block copolypeptides, the $P(BLG_{0.5}$-*r*-$BLT_{0.5})_{1200}$ chains retained an α-helical conformation during hot-pressing at 160 °C (Figure S29b). Despite having a similar molecular weight and composition to the $(PBLG_{200}$-*b*-$PBLT_{200})_3$ films, the random copolypeptide $P(BLG_{0.5}$-*r*-$BLT_{0.5})_{1200}$ exhibited considerably lower ultimate strength and extensibility (Figure S29c). The absence of β-sheet structures in this polymer, crucial for reinforcing mechanical strength, underscores this observation. This control experiment demonstrates that the multiblock architecture, rather than the molecular weight alone, plays a pivotal role in enhancing the mechanical properties of the copolypeptide materials.

Regardless of the types of β-sheet-forming blocks used—PBLT, PVal, or PAla—the ultimate strength measured at 30 °C for our multiblock film samples appears to peak at approximately 30 MPa, with the tensile modulus reaching between 1.5 and 2 GPa (Table 1). These values are on par with most regenerated silk or polypeptide-based mimics of spider silk, typically produced through wet-spinning methods or slow solution casting.[13,17,82,83] In contrast, the thermomechanical processing of our multiblock films is simple, fast and solvent-free, applicable to various β-sheet-forming polypeptide designs. Furthermore, our DMTA measurements on these film samples (Figure S30), specifically $(PBLG_{40}$-*b*-$PVal_{30})_3$, and

https://doi.org/10.1021/jacs.4c10998
J. Am. Chem. Soc. XXXX, XXX, XXX−XXX

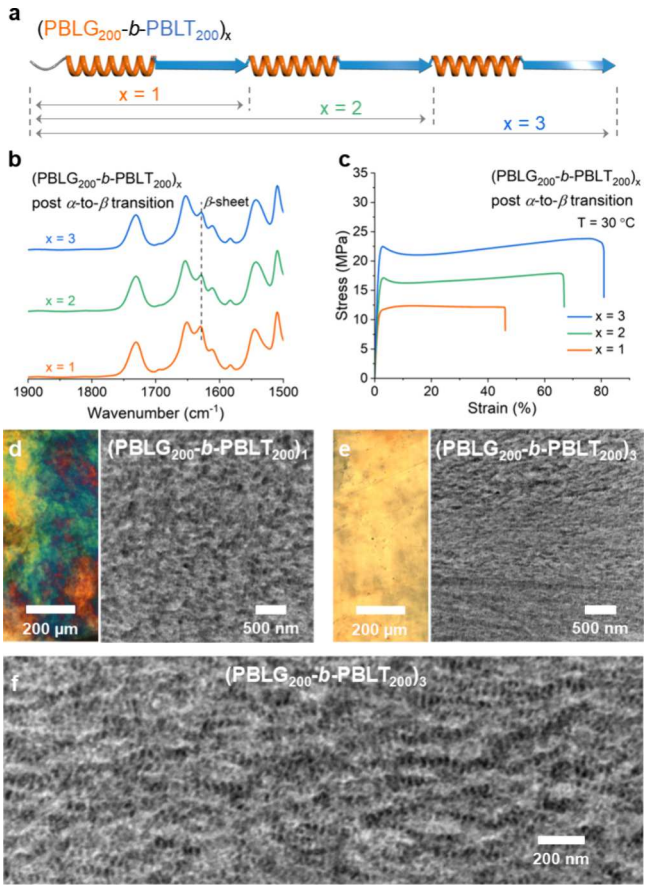

Figure 4. Balancing strength and ductility through copolypeptide compositions. (a) Schematic of the designed $(PBLG_{200}\text{-}b\text{-}PBLT_{200})_x$ multiblock copolypeptides, depicting an increase in the number of repeating blocks. (b) FTIR-ATR spectra of the multiblock copolypeptide films following the in situ α-to-β transition, confirming structural changes. (c) Tensile stress–strain curves of $(PBLG_{200}\text{-}b\text{-}PBLT_{200})_x$ films at 30 °C, highlighting variations in mechanical properties with changes in block numbers. (d, e) POM (left) and TEM (right) images showing the surfaces and microtome-sectioned structures of $(PBLG_{200}\text{-}b\text{-}PBLT_{200})_1$ (d) and $(PBLG_{200}\text{-}b\text{-}PBLT_{200})_3$ (e) films, respectively. (f) High-magnification TEM image of the microtome sections of the $(PBLG_{200}\text{-}b\text{-}PBLT_{200})_3$ film, revealing detailed nanostructures and β-sheet distribution. The films were fabricated through hot-pressing at 160 °C to achieve maximum α-to-β conversion.

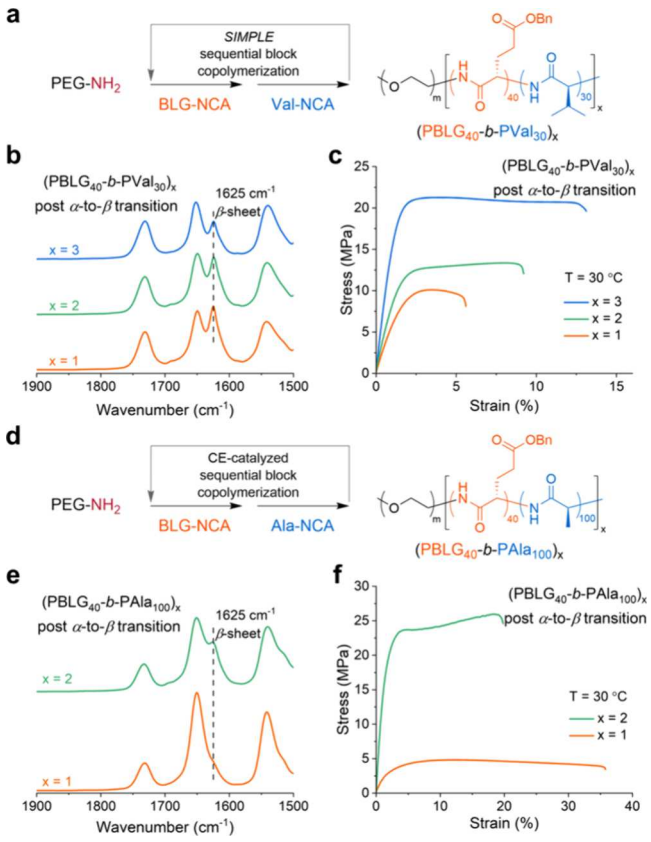

Figure 5. Expanding the amino acid library for multiblock β-sheet materials. Synthetic route of (a) PVal-based multiblock copolypeptides using SIMPLE polymerization methods and (d) PAla-based multiblock copolypeptides using crown ether (CE)-catalyzed polymerization methods. FTIR-ATR spectra of the (b) $(PBLG_{40}\text{-}b\text{-}PVal_{30})_x$ and (e) $(PBLG_{40}\text{-}b\text{-}PAla_{100})_x$ multiblock copolypeptide films with increasing number of repeating blocks after in situ α-to-β transition by annealing. Tensile stress–strain curves for (c) $(PBLG_{40}\text{-}b\text{-}PVal_{30})_x$ and (d) $(PBLG_{40}\text{-}b\text{-}PAla_{100})_x$ films at 30 °C. The films were fabricated through hot-pressing at 200 °C to achieve maximum α-to-β conversion.

$(PBLG_{40}\text{-}b\text{-}PAla_{100})_2$, demonstrate that incorporating different β-sheet-forming amino acids allows for tunability of the modulus at elevated temperatures. Notably, $(PBLG_{40}\text{-}b\text{-}PAla_{100})_2$ maintains a GPa-level storage modulus even when heated to 180 °C. The detailed tensile behaviors of these different β-sheet-forming blocks at elevated temperatures will be discussed in a separate report.

While our film materials currently do not achieve the ultimate strength of natural spider silk, which ranges from 140 to 1500 MPa,[84] largely due to absence of chain orientation and cysteine-based covalent cross-linking, their notable extensibility and adaptability highlight the innovative potential of these copolypeptides with transformable structures. To further enhance their mechanical properties, we experimented with a prestretching technique that applies approximately 70% strain at 100 °C to $(PBLG_{200}\text{-}b\text{-}PBLT_{200})_3$ films, effectively doubling their ultimate tensile strength from 22 to 45 MPa (Figure S31).

POM analysis of the stretched film confirmed the orientation of liquid crystalline domains postdeformation (Figure S32). Additionally, it is well-established that producing thinner fibers can significantly enhance a polymer's strength,[85,86] and evidence suggests that the smaller diameters of spider silk contribute substantially to its exceptional tensile strength.[84] Therefore, it is anticipated that extrusion techniques, which process these transformable copolypeptide materials into fibers, could achieve significant increases in mechanical strength due to the orientation of copolypeptides along the fiber axis and the nature of fracture mechanics.

Our study also demonstrates that moving beyond the natural poly(Ala) constructs found in spider silk, the introduction of novel β-sheet-forming amino acids paves the way for custom-designed copolypeptide mechanical profiles, offering the potential to tailor these materials for targeted functional demands. Future efforts will focus on unraveling the complex relationship between amino acid composition and material properties, their performance at high temperatures, and their ability to mimic the remarkable strain-induced hardening observed in spider-silks. Such insights will likely set the stage for the development of a new class of biomimetic materials suitable for demanding, high-performance applications.

https://doi.org/10.1021/jacs.4c10998
J. Am. Chem. Soc. XXXX, XXX, XXX−XXX

CONCLUSIONS

Inspired by the design principles of spider silk, our study has advanced the development of block copolypeptides that exhibit substantially enhanced mechanical properties. Traditional methods for processing β-sheet structures, like wet spinning or solution casting from regenerated silk, typically require harsh chemicals or involve cumbersome, multistep procedures, creating substantial challenges for scalability and industrial viability. We have overcome these hurdles by employing a novel conformational confinement strategy during β-sheet-forming polypeptide synthesis. This approach enables a controlled α-to-β transition via a straightforward solvent-free, hot processing method, facilitating systematic exploration of spider-silk-like multiblock architectures and the influence of diverse monomeric units on material properties. Our multiblock series, $(PBLG_{200}\text{-}b\text{-}PBLT_{200})_x$, has demonstrated marked improvements in strength and ductility, attributed to an optimized balance of α-helical and β-sheet contents. This optimization has led to significant mechanical enhancements and morphological transformations, highlighting the effectiveness of precise molecular design in tailoring polypeptide properties to meet specific demands.

Furthermore, by employing autoaccelerated helical ROP-NCA polymerization, we have increased the versatility of these synthetic materials by the incorporation of various β-sheet-forming amino acids. The strategic integration of different amino acids has enabled the development of tunable mechanical profiles, expanding the potential applications of our materials. This research represents a step toward bridging the gap between fibrous proteins and synthetic polypeptides—not only mimicking the mechanical properties of biological materials but also extending the capability to tailor them for specialized applications. Future research will aim to further enhance these responsive properties, promoting the emergence of a new class of high-performance, silk-inspired materials the embody the resilience and adaptability of natural spider silk.

ASSOCIATED CONTENT

Supporting Information

The Supporting Information is available free of charge at https://pubs.acs.org/doi/10.1021/jacs.4c10998.

Materials and methods, experimental sections, supplementary figures (Figures S1−S32: characterization of PEG_{113}-PBLG and PEG_{12}-PBLG macroinitiators, FTIR spectra, DSC profiles, DMTA profiles, POM images, deconvolution of amide I peak from the FTIR spectra, summary of the quantitative analysis of β-sheet percentages, XRD profiles, tensile stress−strain curves, WAXS profiles, TEM images, temperature-induced α-to-β transition, conformation and material properties, and enhanced tensile strength), supplementary tables (Tables S1−S3: summary of the synthesis of block copolypeptides, quantitative analysis of the β-sheet percentages present in the copolypeptide materials, and summary of the mechanical properties of $PBLG_{40}$-b-$PBLT_{100}$ materials at 30 °C), and NMR spectra (Figures S33−S46) (PDF)

AUTHOR INFORMATION

Corresponding Authors

Jianjun Cheng − *Department of Chemistry and Department of Materials Science and Engineering, University of Illinois at Urbana−Champaign, Urbana, Illinois 61801, United States;* orcid.org/0000-0003-2561-9291; Email: jianjunc@illinois.edu

Yao Lin − *Polymer Program, Institute of Materials Science and Department of Chemistry, University of Connecticut, Storrs, Connecticut 06269, United States;* orcid.org/0000-0001-5227-2663; Email: yao.lin@uconn.edu

Authors

Tianjian Yang − *Polymer Program, Institute of Materials Science, University of Connecticut, Storrs, Connecticut 06269, United States*

Tianrui Xue − *Department of Chemistry, University of Illinois at Urbana−Champaign, Urbana, Illinois 61801, United States*

Jianan Mao − *Department of Chemistry, University of Connecticut, Storrs, Connecticut 06269, United States*

Stephen R. Ekatan − *Polymer Program, Institute of Materials Science, University of Connecticut, Storrs, Connecticut 06269, United States*

Yingying Chen − *Department of Materials Science and Engineering, University of Illinois at Urbana−Champaign, Urbana, Illinois 61801, United States*

Ziyuan Song − *Jiangsu Key Laboratory for Carbon-Based Functional Materials and Devices, Institute of Functional Nano & Soft Materials (FUNSOM), Soochow University, Suzhou 215123, China;* orcid.org/0000-0002-3165-3712

Complete contact information is available at: https://pubs.acs.org/10.1021/jacs.4c10998

Author Contributions

†T.Y. and T.X. contributed equally to this work.

Notes

The authors declare no competing financial interest.

ACKNOWLEDGMENTS

This work was supported by the NSF grant (DMR 2210590 to Y.L.; CHE-1905097 to J.C.). The authors thank Dr. Hongwei Xia, Prof. Luyi Sun, Prof. Anson Ma, and Prof. Richard Parnas at the UConn Polymer Program for comments and suggestions, Dr. Maritza Abril at the UConn Bioscience Electron Microscopy Lab for TEM characterization, Dr. Dennis Ndaya at the UConn Polymer Program for instrument training, and Prof. Jie Song at UMass Chan Medical School for providing access to the DMTA during our facility's relocation. The LiX beamline is part of the Center for BioMolecular Structure (CBMS), which is primarily supported by the National Institutes of Health, National Institute of General Medical Sciences (NIGMS) through a P30 Grant (P30GM133893), and by the DOE Office of Biological and Environmental Research (KP1605010). LiX also received additional support from NIH Grant S10 OD012331. As part of NSLS-II, a national user facility at Brookhaven National Laboratory, work performed at the CBMS is supported in part by the U.S. Department of Energy, Office of Science, Office of Basic Energy Sciences Program under contract number DE-SC0012704.

REFERENCES

(1) Gosline, J. M.; DeMont, M. E.; Denny, M. W. The structure and properties of spider silk. *Endeavour* **1986**, *10*, 37−43.

(2) Simmons, A. H.; Michal, C. A.; Jelinski, L. W. Molecular orientation and two-component nature of the crystalline fraction of spider dragline silk. *Science* **1996**, *271*, 84−87.
(3) Termonia, Y. Molecular modeling of spider silk elasticity. *Macromolecules* **1994**, *27*, 7378−7381.
(4) Gatesy, J.; Hayashi, C.; Motriuk, D.; Woods, J.; Lewis, R. Extreme diversity, conservation, and convergence of spider silk fibroin sequences. *Science* **2001**, *291*, 2603−2605.
(5) Vollrath, F.; Knight, D. P. Liquid crystalline spinning of spider silk. *Nature* **2001**, *410*, 541−548.
(6) Jin, H. J.; Kaplan, D. L. Mechanism of silk processing in insects and spiders. *Nature* **2003**, *424*, 1057−1061.
(7) Lazaris, A.; Arcidiacono, S.; Huang, Y.; Zhou, J.-F.; Duguay, F.; Chretien, N.; Welsh, E. A.; Soares, J. W.; Karatzas, C. N. Spider silk fibers spun from soluble recombinant silk produced in mammalian cells. *Science* **2002**, *295*, 472−476.
(8) Krejchi, M. T.; Atkins, E. D.; Waddon, A. J.; Fournier, M. J.; Mason, T. L.; Tirrell, D. A. Chemical sequence control of β-sheet assembly in macromolecular crystals of periodic polypeptides. *Science* **1994**, *265*, 1427−1432.
(9) Xia, X.-X.; Qian, Z.-G.; Ki, C. S.; Park, Y. H.; Kaplan, D. L.; Lee, S. Y. Native-sized recombinant spider silk protein produced in metabolically engineered Escherichia coli results in a strong fiber. *Proc. Natl. Acad. Sci. U. S. A.* **2010**, *107*, 14059−14063.
(10) Heidebrecht, A.; Eisoldt, L.; Diehl, J.; Schmidt, A.; Geffers, M.; Lang, G.; Scheibel, T. Biomimetic fibers made of recombinant spidroins with the same toughness as natural spider silk. *Adv. Mater.* **2015**, *27*, 2189−2194.
(11) van Hest, J. C.; Tirrell, D. A. Protein-based materials, toward a new level of structural control. *Chem. Commun.* **2001**, 1897−1904.
(12) Guo, C.; Li, C.; Vu, H. V.; Hanna, P.; Lechtig, A.; Qiu, Y.; Mu, X.; Ling, S.; Nazarian, A.; Lin, S. J.; Kaplan, D. L. Thermoplastic moulding of regenerated silk. *Nat. Mater.* **2020**, *19*, 102−108.
(13) Ling, S.; Qin, Z.; Li, C.; Huang, W.; Kaplan, D. L.; Buehler, M. J. Polymorphic regenerated silk fibers assembled through bioinspired spinning. *Nat. Commun.* **2017**, *8*, 1387.
(14) Yoshioka, T.; Tashiro, K.; Ohta, N. Molecular orientation enhancement of silk by the hot-stretching-induced transition from α-helix-HFIP complex to β-sheet. *Biomacromolecules* **2016**, *17*, 1437−1448.
(15) Omenetto, F. G.; Kaplan, D. L. New opportunities for an ancient material. *Science* **2010**, *329*, 528−531.
(16) Lee, S.-M.; Pippel, E.; Gösele, U.; Dresbach, C.; Qin, Y.; Chandran, C. V.; Bräuniger, T.; Hause, G.; Knez, M. Greatly increased toughness of infiltrated spider silk. *Science* **2009**, *324*, 488−492.
(17) Rathore, O.; Sogah, D. Y. Self-assembly of β-sheets into nanostructures by poly(alanine) segments incorporated in multiblock copolymers inspired by spider silk. *J. Am. Chem. Soc.* **2001**, *123*, 5231−5239.
(18) Yu, T. B.; Bai, J. Z.; Guan, Z. Cycloaddition-Promoted Self-Assembly of a Polymer into Well-Defined β Sheets and Hierarchical Nanofibrils. *Angew. Chem., Int. Ed.* **2009**, *121*, 1117−1121.
(19) Tsuchiya, K.; Numata, K. Chemical Synthesis of Multiblock Copolypeptides Inspired by Spider Dragline Silk Proteins. *ACS Macro Lett.* **2017**, *6*, 103−106.
(20) Croisier, E.; Liang, S.; Schweizer, T.; Balog, S.; Mionić, M.; Snellings, R.; Cugnoni, J.; Michaud, V.; Frauenrath, H. A toolbox of oligopeptide-modified polymers for tailored elastomers. *Nat. Commun.* **2014**, *5*, 4728.
(21) Chan, N. J.-A.; Gu, D.; Tan, S.; Fu, Q.; Pattison, T. G.; O'Connor, A. J.; Qiao, G. G. Spider-silk inspired polymeric networks by harnessing the mechanical potential of β-sheets through network guided assembly. *Nat. Commun.* **2020**, *11*, 1630.
(22) Knowles, T. P. J.; Oppenheim, T. W.; Buell, A. K.; Chirgadze, D. Y.; Welland, M. E. Nanostructured films from hierarchical self-assembly of amyloidogenic proteins. *Nat. Nanotechnol.* **2010**, *5*, 204−7.
(23) Kamada, A.; Rodriguez-Garcia, M.; Ruggeri, F. S.; Shen, Y.; Levin, A.; Knowles, T. P. Controlled self-assembly of plant proteins into high-performance multifunctional nanostructured films. *Nat. Commun.* **2021**, *12*, 3529.
(24) Gu, L.; Jiang, Y.; Hu, J. Scalable Spider-Silk-Like Supertough Fibers using a Pseudoprotein Polymer. *Adv. Mater.* **2019**, *31*, 1904311.
(25) Duraj-Thatte, A. M.; Manjula-Basavanna, A.; Courchesne, N. M.-M. D.; Cannici, G. I.; Sánchez-Ferrer, A.; Frank, B. P.; van't Hag, L.; Cotts, S. K.; Fairbrother, D. H.; Mezzenga, R. Water-processable, biodegradable and coatable aquaplastic from engineered biofilms. *Nat. Chem. Biol.* **2021**, *17*, 732−738.
(26) Ganewatta, M. S.; Wang, Z.; Tang, C. Chemical syntheses of bioinspired and biomimetic polymers toward biobased materials. *Nat. Rev. Chem.* **2021**, *5*, 753−772.
(27) Kushner, A. M.; Guan, Z. Modular design in natural and biomimetic soft materials. *Angew. Chem., Int. Ed.* **2011**, *50*, 9026−9057.
(28) Van Beek, J. D.; Hess, S.; Vollrath, F.; Meier, B. The molecular structure of spider dragline silk: folding and orientation of the protein backbone. *Proc. Natl. Acad. Sci. U. S. A.* **2002**, *99*, 10266−10271.
(29) Holland, G. P.; Creager, M. S.; Jenkins, J. E.; Lewis, R. V.; Yarger, J. L. Determining secondary structure in spider dragline silk by carbon-carbon correlation solid-state NMR spectroscopy. *J. Am. Chem. Soc.* **2008**, *130*, 9871−9877.
(30) Suzuki, Y.; Morie, S.; Okamura, H.; Asakura, T.; Naito, A. Real-Time Monitoring of the Structural Transition of Bombyx mori Liquid Silk under Pressure by Solid-State NMR. *J. Am. Chem. Soc.* **2023**, *145*, 22925−22933.
(31) Keten, S.; Xu, Z.; Ihle, B.; Buehler, M. J. Nanoconfinement controls stiffness, strength and mechanical toughness of B-sheet crystals in silk. *Nat. Mater.* **2010**, *9*, 359−367.
(32) Cranford, S. W.; Tarakanova, A.; Pugno, N. M.; Buehler, M. J. Nonlinear material behaviour of spider silk yields robust webs. *Nature* **2012**, *482*, 72−76.
(33) Meyers, M. A.; McKittrick, J.; Chen, P.-Y. Structural biological materials: critical mechanics-materials connections. *Science* **2013**, *339*, 773−779.
(34) Du, N.; Liu, X. Y.; Narayanan, J.; Li, L.; Lim, M. L. M.; Li, D. Design of superior spider silk: from nanostructure to mechanical properties. *Biophys. J.* **2006**, *91*, 4528−4535.
(35) Liu, Y.; Shao, Z.; Vollrath, F. Relationships between supercontraction and mechanical properties of spider silk. *Nat. Mater.* **2005**, *4*, 901−905.
(36) Krishnaji, S. T.; Bratzel, G.; Kinahan, M. E.; Kluge, J. A.; Staii, C.; Wong, J. Y.; Buehler, M. J.; Kaplan, D. L. Sequence-structure-property relationships of recombinant spider silk proteins: Integration of biopolymer design, processing, and modeling. *Adv. Funct. Mater.* **2013**, *23*, 241−253.
(37) Lefèvre, T.; Rousseau, M.-E.; Pézolet, M. Protein secondary structure and orientation in silk as revealed by Raman spectromicroscopy. *Biophys. J.* **2007**, *92*, 2885−2895.
(38) Deming, T. J. Synthetic polypeptides for biomedical applications. *Prog. Polym. Sci.* **2007**, *32*, 858−875.
(39) Hadjichristidis, N.; Iatrou, H.; Pitsikalis, M.; Sakellariou, G. Synthesis of well-defined polypeptide-based materials via the ring-opening polymerization of α-amino acid N-carboxyanhydrides. *Chem. Rev.* **2009**, *109*, 5528−5578.
(40) Lu, H.; Wang, J.; Song, Z.; Yin, L.; Zhang, Y.; Tang, H.; Tu, C.; Lin, Y.; Cheng, J. Recent advances in amino acid N-carboxyanhydrides and synthetic polypeptides: chemistry, self-assembly and biological applications. *Chem. Commun.* **2014**, *50*, 139−155.
(41) Rodriguez-Hernandez, J.; Chécot, F.; Gnanou, Y.; Lecommandoux, S. Toward 'smart'nano-objects by self-assembly of block copolymers in solution. *Prog. Polym. Sci.* **2005**, *30*, 691−724.
(42) Huang, J.; Heise, A. Stimuli responsive synthetic polypeptides derived from N-carboxyanhydride (NCA) polymerisation. *Chem. Soc. Rev.* **2013**, *42*, 7373−7390.

https://doi.org/10.1021/jacs.4c10998
J. Am. Chem. Soc. XXXX, XXX, XXX−XXX

(43) Baumgartner, R.; Fu, H.; Song, Z.; Lin, Y.; Cheng, J. Cooperative polymerization of α-helices induced by macromolecular architecture. *Nat. Chem.* **2017**, *9*, 614−622.
(44) Song, Z.; Fu, H.; Baumgartner, R.; Zhu, L.; Shih, K.-C.; Xia, Y.; Zheng, X.; Yin, L.; Chipot, C.; Lin, Y.; Cheng, J. Enzyme-mimetic self-catalyzed polymerization of polypeptide helices. *Nat. Commun.* **2019**, *10*, 5470.
(45) Song, Z.; Fu, H.; Wang, J.; Hui, J.; Xue, T.; Pacheco, L. A.; Yan, H.; Baumgartner, R.; Wang, Z.; Xia, Y.; Wang, X.; Yin, L.; Chen, C.; Rodríguez-López, J.; Ferguson, A. L.; Lin, Y.; Cheng, J. Synthesis of polypeptides via bioinspired polymerization of in situ purified N-carboxyanhydrides. *Proc. Natl. Acad. Sci. U. S. A.* **2019**, *116*, 10658−10663.
(46) Wang, X.; Song, Z.; Tan, Z.; Zhu, L.; Xue, T.; Lv, S.; Fu, Z.; Zheng, X.; Ren, J.; Cheng, J. Facile synthesis of helical multiblock copolypeptides: minimal side reactions with accelerated polymerization of N-carboxyanhydrides. *ACS Macro Lett.* **2019**, *8*, 1517−1521.
(47) Zou, J.; Fan, J.; He, X.; Zhang, S.; Wang, H.; Wooley, K. L. A facile glovebox-free strategy to significantly accelerate the syntheses of well-defined polypeptides by N-carboxyanhydride (NCA) ring-opening polymerizations. *Macromolecules* **2013**, *46*, 4223−4226.
(48) Grazon, C.; Salas-Ambrosio, P.; Ibarboure, E.; Buol, A.; Garanger, E.; Grinstaff, M. W.; Lecommandoux, S.; Bonduelle, C. Aqueous ring-opening polymerization-induced self-assembly (ROPISA) of N-carboxyanhydrides. *Angew. Chem., Int. Ed.* **2020**, *132*, 632−636.
(49) Murphy, R. D.; Garcia, R. V.; Oh, S. J.; Wood, T. J.; Jo, K. D.; Read de Alaniz, J.; Perkins, E.; Hawker, C. J. Tailored polypeptide star copolymers for 3D printing of bacterial composites Via direct ink writing. *Adv. Mater.* **2023**, *35*, 2207542.
(50) Wang, S.; Lu, M.-Y.; Wan, S.-K.; Lyu, C.-Y.; Tian, Z.-Y.; Liu, K.; Lu, H. Precision Synthesis of Polysarcosine via Controlled Ring-Opening Polymerization of N-Carboxyanhydride: Fast Kinetics, Ultrahigh Molecular Weight, and Mechanistic Insights. *J. Am. Chem. Soc.* **2024**, *146*, 5678−5692.
(51) Fu, H.; Baumgartner, R.; Song, Z.; Chen, C.; Cheng, J.; Lin, Y. Generalized model of cooperative covalent polymerization: connecting the supramolecular binding interactions with the catalytic behavior. *Macromolecules* **2022**, *55*, 2041−2050.
(52) Mondeshki, M.; Spiess, H. W.; Aliferis, T.; Iatrou, H.; Hadjichristidis, N.; Floudas, G. Hierarchical self-assembly in diblock copolypeptides of poly (γ-benzyl-L-glutamate) with poly poly (L-leucine) and poly (O-benzyl-L-tyrosine). *Eur. Polym. J.* **2011**, *47*, 668−674.
(53) Robinson, C. Liquid-crystalline structures in solutions of a polypeptide. *Trans. Faraday Soc.* **1956**, *52*, 571−592.
(54) Samulski, E.; Tobolsky, A. Solid "liquid crystal" films of poly-γ-benzyl-L-glutamate. *Nature* **1967**, *216*, 997−997.
(55) Ekatan, S. R.; Xue, T.; Song, Z.; Yang, T.; Ndaya, D.; Shaw, M. T.; Cheng, J.; Lin, Y. Thermomechanical Properties of Solid "Liquid Crystalline" Films from Hot-Pressed Synthetic Polypeptides of Various Macromolecular Architectures. *Macromolecules* **2024**, *57*, 2008−2018.
(56) Kricheldorf, H. R.; von Lossow, C.; Schwarz, G. Primary Amine-Initiated Polymerizations of Alanine-NCA and Sarcosine-NCA. *Macromol. Chem. Phys.* **2004**, *205*, 918−924.
(57) Gitsas, A.; Floudas, G.; Mondeshki, M.; Spiess, H. W.; Aliferis, T.; Iatrou, H.; Hadjichristidis, N. Control of peptide secondary structure and dynamics in poly (γ-benzyl-l-glutamate)-b-polyalanine peptides. *Macromolecules* **2008**, *41*, 8072−8080.
(58) Koenig, J.; Sutton, P. Raman scattering of some synthetic polypeptides: Poly (γ-benzyl L-glutamate), poly-L-leucine, poly-L-valine, and poly-L-serine. *Biopolymers* **1971**, *10*, 89−106.
(59) Blout, E. R.; Lenormant, H. Reversible configurational changes in poly-L-lysine hydrochloride induced by water. *Nature* **1957**, *179*, 960−963.
(60) Bamford, C. H.; Hanby, W.; Happey, F. The structure of synthetic polypeptides I. *X-ray investigation. Proc. R. Soc. London A. Math. Phys. Sci.* **1951**, *205*, 30−47.
(61) Bamford, C. H. *Synthetic Polypeptides: Preparation, Structure, and Properties*; Academic Press, 1956.
(62) Bamford, C.; Brown, L.; Elliott, A.; Hanby, W. E.; Trotter, I. Alpha-and beta-forms of poly-L-alanine. *Nature* **1954**, *173*, 27−29.
(63) Elliott, A.; Hanby, W.; Malcolm, B. The near infra-red absorption spectra of natural and synthetic fibres. *Br. J. Appl. Phys.* **1954**, *5*, 377.
(64) Henzler Wildman, K. A.; Lee, D. K.; Ramamoorthy, A. Determination of α-helix and β-sheet stability in the solid state: a solid-state NMR investigation of poly (L-alanine). *Biopolymers* **2002**, *64*, 246−254.
(65) Gibson, M. I.; Cameron, N. R. Organogelation of sheet−helix diblock copolypeptides. *Angew. Chem., Int. Ed.* **2008**, *120*, 5238−5240.
(66) Fan, J.; Zou, J.; He, X.; Zhang, F.; Zhang, S.; Raymond, J. E.; Wooley, K. L. Tunable mechano-responsive organogels by ring-opening copolymerizations of N-carboxyanhydrides. *Chem. Sci.* **2014**, *5*, 141−150.
(67) Nisal, R.; Jayakannan, M. Tertiary-Butylbenzene Functionalization as a Strategy for β-Sheet Polypeptides. *Biomacromolecules* **2022**, *23*, 2667−2684.
(68) Xue, T.; Song, Z.; Wang, Y.; Zhu, B.; Zhao, Z.; Tan, Z.; Wang, X.; Xia, Y.; Cheng, J. Streamlined synthesis of PEG-polypeptides directly from amino acids. *Macromolecules* **2020**, *53*, 6589−6597.
(69) Yang, T.; Xue, T.; Mao, J.; Chen, Y.; Tian, H.; Bartolome, A.; Xia, H.; Yao, X.; Kumar, C. V.; Cheng, J. Tailoring Synthetic Polypeptide Design for Directed Fibril Superstructure Formation and Enhanced Hydrogel Properties. *J. Am. Chem. Soc.* **2024**, *146*, 5823−5833.
(70) Green, M. M.; Reidy, M. P.; Johnson, R. D.; Darling, G.; O'Leary, D. J.; Willson, G. Macromolecular stereochemistry: the out-of-proportion influence of optically active comonomers on the conformational characteristics of polyisocyanates. The sergeants and soldiers experiment. *J. Am. Chem. Soc.* **1989**, *111*, 6452−6454.
(71) Schenning, A.; Kilbinger, A.; Biscarini, F.; Cavallini, M.; Cooper, H.; Derrick, P.; Feast, W.; Lazzaroni, R.; Leclere, P.; McDonell, L. Supramolecular organization of α, α'-disubstituted sexithiophenes. *J. Am. Chem. Soc.* **2002**, *124*, 1269−1275.
(72) Smulders, M. M.; Schenning, A. P.; Meijer, E. Insight into the mechanisms of cooperative self-assembly: The "sergeants-and-soldiers" principle of chiral and achiral C3-symmetrical discotic triamides. *J. Am. Chem. Soc.* **2008**, *130*, 606−611.
(73) Pielichowski, K.; Flejtuch, K. Differential scanning calorimetry studies on poly (ethylene glycol) with different molecular weights for thermal energy storage materials. *Polym. Adv. Technol.* **2002**, *13*, 690−696.
(74) Craig, D.; Newton, J. Characterisation of polyethylene glycols using differential scanning calorimetry. *Int. J. Pharm.* **1991**, *74*, 33−41.
(75) Fukuzawa, T.; Uematsu, I.; Uematsu, Y. Viscoelastic Properties of Poly (γ-benzyl glutamate). *Polym. J.* **1974**, *6*, 431−437.
(76) McKinnon, A. J.; Tobolsky, A. V. Structure and properties of poly (. gamma.-benzyl-L-glutamate) cast from dimethylformamide. *J. Phys. Chem.* **1968**, *72*, 1157−1161.
(77) Lee, N. H.; Frank, C. W. Surface-initiated vapor polymerization of various α-amino acids. *Langmuir* **2003**, *19*, 1295−1303.
(78) Parry, D.; Elliott, A. X-ray Diffraction Patterns of Liquid Crystalline Solutions of Poly-γ-benzyl-L-glutamate. *Nature* **1965**, *206*, 616−617.
(79) Watanabe, J.; Imai, K.; Gehani, R.; Uematsu, I. Structural differences between two crystal modifications of poly (γ-benzyl l-glutamate). *J. Polym. Sci., Part B: Polym. Phys.* **1981**, *19*, 653−665.
(80) Fändrich, M.; Dobson, C. M. The behaviour of polyamino acids reveals an inverse side chain effect in amyloid structure formation. *EMBO J.* **2002**, *21*, 5682−5690.
(81) Grubb, D. T.; Jelinski, L. W. Fiber morphology of spider silk: the effects of tensile deformation. *Macromolecules* **1997**, *30*, 2860−2867.

https://doi.org/10.1021/jacs.4c10998
J. Am. Chem. Soc. XXXX, XXX, XXX−XXX

(82) Marelli, B.; Patel, N.; Duggan, T.; Perotto, G.; Shirman, E.; Li, C.; Kaplan, D. L.; Omenetto, F. Programming function into mechanical forms by directed assembly of silk bulk materials. *Proc. Natl. Acad. Sci. U. S. A.* **2017**, *114*, 451−456.
(83) An, B.; Jenkins, J. E.; Sampath, S.; Holland, G. P.; Hinman, M.; Yarger, J. L.; Lewis, R. Reproducing natural spider silks' copolymer behavior in synthetic silk mimics. *Biomacromolecules* **2012**, *13*, 3938−3948.
(84) Yarger, J. L.; Cherry, B. R.; Van Der Vaart, A. Uncovering the structure-function relationship in spider silk. *Nat. Rev. Mater.* **2018**, *3*, 8000.
(85) Porter, D.; Guan, J.; Vollrath, F. Spider silk: super material or thin fibre? *Adv. Mater.* **2013**, *9*, 1275−1279.
(86) Guan, J.; Porter, D.; Vollrath, F. Silks cope with stress by tuning their mechanical properties under load. *Polymer* **2012**, *53*, 2717−2726.

https://doi.org/10.1021/jacs.4c10998
J. Am. Chem. Soc. XXXX, XXX, XXX−XXX